

## Position Control of a Pneumatic Actuator Under Varying External Force

Eddie ZISSER and Avishai SINTOV and Amir SHAPIRO

*Department of Mechanical Engineering, Ben-Gurion University of the Negev, Beer-Sheva, Israel  
sintova@post.bgu.ac.il*

Raziel RIEMER

*Department of Industrial and Management Engineering, Ben-Gurion University of the Negev,  
Beer-Sheva, Israel*

Received (28 September 2017)

Revised (12 March 2018)

Accepted (20 November 2018)

In this paper a high accuracy position control strategy for a pneumatic actuation system subjected to a varying external force is proposed. A novel approach for the mathematical modeling of the pneumatic actuator, based on energy methods, is presented. The Lagrangian is derived from combining the kinetic and potential energies, leading to formulation of the Euler-Lagrange equation of motion. The nonlinear backstepping method is applied to derive the control law, and the derivative of the potential energy is used as the controlled parameter. Experimental results show that tracking a sine wave of 0.1m magnitude produces a maximum error of  $\pm 0.008\text{m}$  while the actuator is subjected to a time varying external force with a magnitude ranging from 570N to 1150N.

*Keywords:* Pneumatic actuator, Euler-Lagrange equation of motion, nonlinear position control, external force.

### 1. Introduction

Pneumatic actuation systems have been a controversial subject for years in the fields of automation and industrial control. The main advantages of pneumatic actuation systems, such as high power to weight ratio, cleanliness, low cost, reliability and simplicity, have contributed to their widespread use, especially for implementation in automated production lines and industrial tools. On the other hand, the compressibility of the working media (usually air) makes it difficult to accurately predict their dynamic behavior. This disadvantage has limited the implementation of pneumatic actuators to open-loop applications, where accurate motion is not required.

The first attempt to use a closed-loop controlled pneumatic system was published by Shearer [1]. His work included a theoretical analysis of the pneumatic actuator and the control valve. Based on a linearized dynamic model, he proposed a control strategy that could stabilize the system at the equilibrium point. However, this control approach is valid only in the vicinity of the equilibrium point. Nevertheless, this modeling methodology became the conventional modeling approach were the mass flow-rate passing through the valve is integrated into the actuator's dynamic model, which is defined by Newton's second law. Later studies improved Shearer's work by modeling the system with more details, i.e. considering more physical phenomena, increasing the depth in which the phenomena are portrayed, and reevaluating the simplifying assumptions. For example, the extensive dynamic model of Richer and Hurmuzlu [2], which includes the effects of nonlinear flow through the valve and air compressibility in the actuator's chambers and also considers the leakage between chambers, the end of stroke inactive volume, the time delay and attenuation in the pneumatic lines.

Solution for the control problem of pneumatic systems can be achieved using various methods, where the main control objectives are position and velocity tracking. Preceding papers, such as [3–5], proposed classical control strategies that were applied to a linearized dynamic model of the pneumatic system. In the last two decades, we have witnessed growing interest in nonlinear control theory and the implementation of nonlinear control techniques to pneumatics. The backstepping methodology was proposed in [6] and [7], while other researchers, as reported in [8–10] used the sliding mode control method. A combination of backstepping with sliding mode was used in [11] and [12], while [13] described the design of an H-infinity controller for an artificial pneumatic muscle.

In this paper we propose a new approach for the modeling and control of a pneumatic actuation system subjected to an external force. In Sec. 2, we derive the actuator's dynamic model based on the Lagrangian mechanics principles instead of using the traditional force analysis. The modeling was performed as follows: first we defined the kinetic energy and the potential energy, then we formulated the Lagrangian of the actuator and, finally, we developed the equation of motion of the system. In Secs. 3 and 4 we apply the nonlinear backstepping method, by using the derivative of the potential energy as the controlled parameter, to track a reference position trajectory. In the following section we also mathematically prove that the controlled system is asymptotically stable. Further, in Sec. 5, we analyze of the dynamic model by simulation. Finally, in Sec. 6 we demonstrate the performance of our new approach by implementing the control law in an experiment setup, in which the actuator is disturbed by a varying external force.

## **2. The Dynamic Model**

The pneumatic actuation system (Fig. 1) is composed of five basic elements: an actuator, a control valve, a pneumatic source of compressed air, measuring equipment ((a) measures the travel distance and (b) are two pressure sensors) and a micro-controller for computation and data acquisition.

The pneumatic actuator transforms pneumatic energy to mechanical energy. It comprises a cylinder, a piston which separates the inner volume into two chambers,

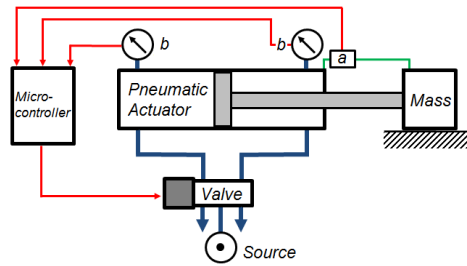


Figure 1 Pneumatic actuation system scheme

and two ports at the ends of the cylinder that allow air charge or discharge from the chambers. Changing the mass of air in the chamber changes the pressure, and thus changes the net force acting on the piston, therefore causing movement of the piston and the rod connected to it. Notations that describe the actuator are shown in Fig. 2, where  $i = 1$  corresponds to the left chamber and  $i = 2$  to the right chamber.

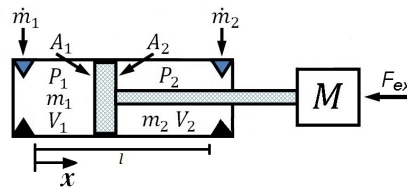


Figure 2 A schematic illustration of the pneumatic actuator

That is,  $\dot{m}_i$  is the inlet or outlet mass flow-rate through the port of chamber  $i$ ,  $A_i$  is the piston's cross section area,  $P_i$  is the pressure,  $m_i$  is the mass of air and  $V_i$  is the volume. In addition,  $F_{ex}$  is the external force,  $x$  is the position of the piston,  $l$  is the piston's stroke and  $M$  is the total mass of the piston, the rod and the external mass. This model also includes a 'dead volume', which is the remaining volume when the piston reaches the end of its stroke. The two lower black triangles at the ends of the cylinder indicate the 'dead volume', while the two upper triangles represent the inlet/outlet ports.

### 2.1. The Energy of the Actuator

In order to describe the dynamics of the actuator in terms of energy, we apply the principles of Lagrangian mechanics. We introduce the Lagrangian of the actuator,  $\mathcal{L}$ , which is defined as the difference between the total kinetic energy,  $\mathcal{T}$ , associated with inertia and movement of masses and the total potential energy,  $\mathcal{V}$ , associated with the energy content of the substance and of its pressure and volume. Hence,

$$\mathcal{L} = \mathcal{T} - \mathcal{V}. \tag{1}$$

The kinetic energy of the actuator,  $\mathcal{T}$ , is associated with the total mass of all moving parts (piston, rod and external mass). The kinetic energy is defined such

that

$$\mathcal{T} = \frac{1}{2}M\dot{x}^2, \quad (2)$$

where  $M$  is the total moving mass and  $\dot{x}$  is the time derivative of the position  $x$ , i.e., the velocity of the mass.

Pneumatic potential energy is the energy stored in pressurized compressible fluids. In order to determine the potential energy of the actuator we need to define the relation between the force and the generalized displacement. We adopt the approach by which, in a pneumatic domain, the pressure is analogous to the force and the volume is analogous to the displacement [14].

**The relation between pressure and volume:** We use the case of a sealed cylinder with varying volume (Fig. 3) to describe this relation.

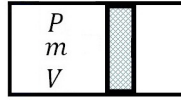


**Figure 3** Varying volume chamber and movable piston

The chamber is sealed by the cylinder walls and a movable piston.  $P$ ,  $m$  and  $V$  are the air pressure inside the chamber, the mass of air in the chamber and the volume of the chamber, respectively. Assuming the air behaves as an ideal gas, the relation between pressure and volume is defined by the ideal gas law:

$$PV = mRT, \quad (3)$$

where  $R$  is the specific gas constant of air and  $T$  is the air temperature.

**Potential energy of a varying volume chamber:** We assume that the thermodynamic process is isothermal, i.e. the air temperature does not change. An incremental amount of work done by the pressure is defined by

$$PdV = \frac{mRT}{V}dV, \quad (4)$$

and the total work done by the pressure,  $W$ , is calculated by the integral

$$W = - \int_{V_0}^V PdV = -mRT \ln \left( \frac{V}{V_0} \right), \quad (5)$$

where  $V_0$  is the initial volume of the chamber. In fact, (5) is the potential energy of the closed chamber.<sup>1</sup>

**Potential energy of the actuator:** The potential energy of the actuator,  $\mathcal{V}$ , is defined as the energy content of the mass of the substance (air) inside the actuators chambers and its thermodynamic properties.

<sup>1</sup>The minus sign in (5) is a result of a sign convention by which mechanical work done by the system on the surroundings is considered to be negative.

Once we know the potential energy of a varying volume chamber we can model the actuator as two connected chambers, divided by the piston, as shown in Fig. 4. The potential energy of the actuator,  $\mathcal{V}$ , is a function of the chambers' volumes. That is

$$\mathcal{V}(V_1, V_2) = -RT \left( m_1 \ln \left( \frac{V_1}{V_{0,1}} \right) + m_2 \ln \left( \frac{V_2}{V_{0,2}} \right) \right), \quad (6)$$

where  $m_i$ ,  $V_i$  and  $V_{0,i}$  are the mass of air, the volume chamber  $i$  and its initial volume, respectively. We define the initial volume as the 'dead volume' of the actuator. Since the 'dead volume' is reported as equal for both chambers, it is denoted in the rest of this paper by  $V_0$ .

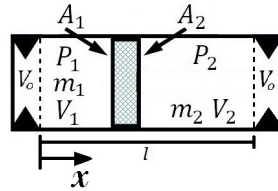


**Figure 4** Closed container separated into two chambers by a piston

The geometric relation between the volumes and the pistons position is

$$V_1 = A_1 x \quad (7)$$

$$V_2 = A_2 (l - x). \quad (8)$$

Thus,

$$\mathcal{V}(x) = -RT \left( m_1 \ln \left( \frac{A_1 x}{V_0} \right) + m_2 \ln \left( \frac{A_2 (l - x)}{V_0} \right) \right). \quad (9)$$

In a closed container the masses,  $m_1$  and  $m_2$ , are constants, and thus the potential energy is dependent only on the displacement of the piston,  $x$ . The real actuator, on the other hand, is not sealed and  $m_1$  and  $m_2$  can be changed at any time by inlet or outlet flow. However, since the system was designed with pressure gauges that measure the pressures in the actuators chambers, we use the ideal gas law, (3), to calculate  $m_1$  and  $m_2$ . Hence,  $\mathcal{V}$  can represent the potential energy of the real actuator.

## 2.2. The Equation of Motion of the Actuator

Using the the kinetic energy (2) and the potential energy (9) of the actuator as a function of the piston position and velocity, we can now write the Lagrangian (1) as

$$\mathcal{L}(x, \dot{x}) = \frac{1}{2} M \dot{x}^2 - RT \left( m_1 \ln \left( \frac{A_1 x}{V_0} \right) + m_2 \ln \left( \frac{A_2 (l - x)}{V_0} \right) \right). \quad (10)$$

The Euler-Lagrange equation of motion for a non conservative system is

$$\frac{d}{dt} \left( \frac{\partial \mathcal{L}}{\partial \dot{x}} \right) - \frac{\partial \mathcal{L}}{\partial x} = - \frac{\partial \mathcal{F}}{\partial \dot{x}} \quad (11)$$

where  $\frac{\partial \mathcal{F}}{\partial \dot{x}}$  is the partial derivative of the energy dissipation,  $\mathcal{F}$ , with respect to the velocity  $\dot{x}$ . The energy dissipation in the actuator is due to work done by the friction force. Therefore,  $\frac{\partial \mathcal{F}}{\partial \dot{x}} = F_f$ , where  $F_f$  is the friction force caused by the seals of the piston and the rod. For simplicity we adopt the continuous linear model of viscous friction. That is

$$F_f(\dot{x}) = \mu_v \dot{x}, \quad (12)$$

where  $\mu_v$  is the viscous friction coefficient. From experiment,  $\mu_v$  is estimated to be 200 kg/s. Calculating the derivatives of (11), results in

$$M\ddot{x} - RT \left( \frac{m_1}{x} - \frac{m_2}{l-x} \right) = -\mu_v \dot{x}, \quad (13)$$

which is the equation of motion of the actuator.

### 3. State Space Formulation

#### 3.1. Single Integrator Form

The state space representation of (13) is

$$\dot{x}_1 = x_2 \quad (14)$$

$$\dot{x}_2 = \frac{1}{M} \left( RT \left( \frac{m_1}{x_1} - \frac{m_2}{l-x_1} \right) - \mu_v x_2 \right). \quad (15)$$

We denote the first term on the right side of (15)

$$\zeta = RT \left( \frac{m_1}{x_1} - \frac{m_2}{l-x_1} \right), \quad (16)$$

which gives

$$\dot{x}_1 = x_2 \quad (17)$$

$$\dot{x}_2 = \frac{1}{M} (\zeta - \mu_v x_2). \quad (18)$$

Notice that system (17)–(18) describes the dynamics of the actuator for fixed masses of air in the actuator's chambers,  $m_1$  and  $m_2$ . Using the pneumatic valve, which is connected to the actuator's ports, we control the actuator by changing  $m_1$  and  $m_2$ . Thus,  $\zeta$  is a function of the time dependent parameters  $x_1(t)$ ,  $m_1(t)$  and  $m_2(t)$ . In order to include the changes of the masses in the dynamic model, we differentiate  $\zeta$  with respect to the time,

$$\begin{aligned} \frac{d\zeta}{dt} &= \frac{\partial \zeta}{\partial x_1} \frac{dx_1}{dt} + \frac{\partial \zeta}{\partial m_1} \frac{dm_1}{dt} + \frac{\partial \zeta}{\partial m_2} \frac{dm_2}{dt} = \\ &= RT \left( \frac{\dot{m}_1}{x_1} - \frac{\dot{m}_2}{l-x_1} - x_2 \left( \frac{m_1}{x_1^2} + \frac{m_2}{(l-x_1)^2} \right) \right), \end{aligned} \quad (19)$$

where  $\dot{m}_1$  and  $\dot{m}_2$  are the mass flow-rate of air entering and exiting the chambers of the actuator. The mass flow-rate is the input to the actuator and is controlled

by the input to the valve. In this paper, we use a linear model to describe the mass flow-rate through the valve:

$$\dot{m}_1 = \alpha_1 u_V + \beta_1 \tag{20}$$

$$\dot{m}_2 = -\alpha_2 u_V + \beta_2, \tag{21}$$

where  $\alpha_1, \alpha_2, \beta_1$  and  $\beta_2$  are all scalars and  $u_V$  is the input voltage of the valve. Choosing

$$u_V = \frac{1}{\frac{\alpha_1}{x_1} + \frac{\alpha_2}{l-x_1}} \left( -\frac{\beta_1}{x_1} + \frac{\beta_2}{l-x_1} + x_2 \left( \frac{m_1}{x_1^2} + \frac{m_2}{(l-x_1)^2} \right) + \frac{u}{RT} \right), \tag{22}$$

and substituting equations (20)–(22) to (19) yields the three-equation system

$$\dot{x}_1 = x_2 \tag{23}$$

$$\dot{x}_2 = \frac{1}{M} (\zeta - \mu_v x_2) \tag{24}$$

$$\dot{\zeta} = u \tag{25}$$

where  $u$  is the control input.

The backstepping algorithm is designed to be applied on systems of the single integrator form. We further seek to represent system (23)–(25) in the single integrator form. To this end, we define the vector  $\mathbf{X} = [x_1, x_2]^T$ . Further, we define functions  $f : D \rightarrow \mathbb{R}^2$  and  $g : D \rightarrow \mathbb{R}^2$  that are smooth in a domain  $D \in \mathbb{R}^2$  which contains  $\mathbf{X} = \mathbf{0}$  with  $f(\mathbf{0}) = \mathbf{0}$  and  $g(\mathbf{X}) \neq \mathbf{0}$ . Choosing

$$f(\mathbf{X}) = \begin{bmatrix} x_2 \\ -\frac{\mu_v}{M} x_2 \end{bmatrix} \text{ and } g(\mathbf{X}) = \begin{bmatrix} 0 \\ \frac{1}{M} \end{bmatrix} \tag{26}$$

transforms system (23)–(25) into the single integrator form

$$\dot{\mathbf{X}} = f(\mathbf{X}) + g(\mathbf{X}) \zeta \tag{27}$$

$$\dot{\zeta} = u, \tag{28}$$

where  $[\mathbf{X}^T, \zeta]^T \in \mathbb{R}^3$  is the state vector and  $u \in \mathbb{R}$  is the control input.

### 3.2. Tracking Error

We aim to design a controller to drive the actuator and asymptotically track a bounded reference position signal  $x_d$ , which is assumed to be a continuous and differentiable smooth signal. Thus, we define a new state vector  $[\mathbf{X}_e, \zeta_e]^T = [x_{e1}, x_{e2}, \zeta_e]^T$ , which represents the tracking error, such that

$$x_{e1} = x_1 - x_d \tag{29}$$

$$x_{e2} = x_2 - \dot{x}_d \tag{30}$$

$$\zeta_e = \zeta - \dot{\zeta}_d, \tag{31}$$

where  $\dot{x}_d$  is the time derivative of  $x_d$ , and the  $\zeta$  error  $\zeta_d$  is defined by

$$\zeta_d = \frac{RT}{M} \left( \frac{m_1}{x_d} - \frac{m_2}{l-x_d} \right). \tag{32}$$

By differentiating (29)–(31) we get  $\dot{x}_{e1} = \dot{x}_1 - \dot{x}_d$ ,  $\dot{x}_{e2} = \dot{x}_2 - \dot{x}_d$ , and  $\dot{\zeta}_e = \dot{\zeta} - \dot{\zeta}_d$ . We can now write

$$\dot{\mathbf{X}}_e = f(\mathbf{X}) + g(\mathbf{X})\zeta - \begin{bmatrix} \dot{x}_d \\ \ddot{x}_d \end{bmatrix} = \begin{bmatrix} x_2 - \dot{x}_d \\ -\frac{\mu_v}{M}x_2 - \ddot{x}_d \end{bmatrix} + \begin{bmatrix} 0 \\ \frac{1}{M} \end{bmatrix} \zeta. \quad (33)$$

Since  $\dot{x}_1 = x_2$  and assuming  $\ddot{x}_d = 0$ , we get

$$\dot{\mathbf{X}}_e = f(\mathbf{X}_e) + g(\mathbf{X}_e)\zeta.$$

Thus, replacing the state vector  $[\mathbf{X}, \zeta]^T$  with  $[\mathbf{X}_e, \zeta_e]^T$  in system (27)–(28) gives

$$\dot{\mathbf{X}}_e = f(\mathbf{X}_e) + g(\mathbf{X}_e)\zeta_e \quad (34)$$

$$\dot{\zeta}_e = u. \quad (35)$$

System (34)–(35) relaxes all the previous requirements, and for the input  $u = 0$  the system has an equilibrium point at  $[\mathbf{X}_e, \zeta_e]^T = \mathbf{0}$ .

#### 4. Position Control of the Actuator

In this chapter we derive the control law, using the backstepping algorithm.

**Claim 1.** *Given system (34)–(35), where the state vector  $[\mathbf{X}_e, \zeta_e]^T$  is defined by (29)–(31), the state feedback control law*

$$u = -2x_{e2} + k_1 \left( \frac{\mu_v}{M} x_{e2} - \zeta_e \right) - k_2 (\zeta_e + x_{e1} + k_1 x_{e2}), \quad (36)$$

for positive definite  $k_1$  and  $k_2$ , asymptotically stabilizes the system at the origin  $[\mathbf{X}_e, \zeta_e]^T = \mathbf{0}$ . That is,  $u$  forces the system to track the reference position trajectory  $x_d$ .

*Proof.* The backstepping procedure starts by considering (34). We wish to design a state feedback control law  $\zeta = \varphi(\mathbf{X}_e)$  in order to asymptotically stabilize

$$\dot{\mathbf{X}}_e = f(\mathbf{X}_e) + g(\mathbf{X}_e)\varphi \quad (37)$$

at the origin,  $\mathbf{X}_e = \mathbf{0}$  ( $\varphi(\mathbf{X}_e)$  is denoted  $\varphi$  for brevity). For this purpose we use the direct Lyapunov method, i.e., we look for a certain positive definite function  $V(\mathbf{X}_e)$ . The derivative of  $V(\mathbf{X}_e)$  along the trajectories of the subsystem (37) must be negative definite. That is,  $\dot{V}$  must satisfy

$$\begin{aligned} \dot{V} &= \frac{\partial V}{\partial \mathbf{X}_e} (f(\mathbf{X}_e) + g(\mathbf{X}_e)\varphi) < 0 \\ \text{for } \mathbf{X}_e &\in D, \end{aligned} \quad (38)$$

and

$$\dot{V}(\mathbf{0}) = 0. \quad (39)$$

Choosing a candidate Lyapunov function  $V(\mathbf{X}_e)$  such that

$$V(\mathbf{X}_e) = \frac{1}{2} \mathbf{X}_e^T \mathbf{X}_e \quad (40)$$

yields

$$\dot{V}(\mathbf{X}_e) = x_{e1}x_{e2} - \frac{\mu_v}{M}x_{e2}^2 + x_{e2}\varphi. \tag{41}$$

If we further choose

$$\varphi = -x_{e1} - k_1x_{e2}, \tag{42}$$

where  $k_1$  is a positive scalar, and then, substitute (42) into (41), we get

$$\dot{V}(\mathbf{X}_e) = -x_{e2}^2 \left( \frac{\mu_v}{M} + k_1 \right). \tag{43}$$

Considering (43), we notice that  $\dot{V}(\mathbf{X}_e)$  is independent of  $x_{e1}$ . Thus,

$$\dot{V}(\mathbf{X}_e) \leq 0$$

in  $\mathbf{X}_e \in D$  and criterion (38) is not satisfied. Nevertheless, it is clear that  $\dot{V}(\mathbf{X}_e)$  is negative everywhere except on the line  $x_{e2} = 0$  (i.e.,  $\dot{V}(x_{e1}, x_{e2} = 0) = 0$ ). Rewriting (37) after substitution from (26) and (42) yields

$$\dot{\mathbf{X}}_e = \begin{bmatrix} x_{e2} \\ -\frac{\mu_v}{M}x_{e2} \end{bmatrix} + \begin{bmatrix} 0 \\ \frac{1}{M} \end{bmatrix} (-x_{e1} - k_1x_{e2}).$$

We notice that the subsystem can maintain the state  $\dot{\mathbf{X}}_e = 0$  only at the origin  $\mathbf{X}_e = \mathbf{0}$ . Therefore, by following LaSalle’s invariance principle, we conclude that the origin is asymptotically stable. Adding and subtracting  $g(\mathbf{X}_e)\varphi$  on the right-hand side of (34), we obtain the equivalent representation:

$$\dot{\mathbf{X}}_e = (f(\mathbf{X}_e) + g(\mathbf{X}_e)\varphi) + g(\mathbf{X}_e)(\zeta_e - \varphi) \tag{44}$$

$$\dot{\zeta}_e = u. \tag{45}$$

The change of variables

$$z = \zeta_e - \varphi \tag{46}$$

results in the system

$$\dot{\mathbf{X}}_e = (f(\mathbf{X}_e) + g(\mathbf{X}_e)\varphi) + g(\mathbf{X}_e)z \tag{47}$$

$$\dot{z} = u - \dot{\varphi}, \tag{48}$$

where

$$\dot{\varphi} = \frac{\partial \varphi}{\partial \mathbf{X}_e} (f(\mathbf{X}_e) + g(\mathbf{X}_e)\zeta_e). \tag{49}$$

Substituting (26) and (42) gives

$$\dot{\varphi} = -x_{e2} + k_1 \left( \frac{\mu_v}{M}x_{e2} - \zeta_e \right). \tag{50}$$

By taking  $v = u - \dot{\varphi}$ , we reduce the system (47)–(48) to

$$\dot{\mathbf{X}}_e = (f(\mathbf{X}_e) + g(\mathbf{X}_e)\varphi) + g(\mathbf{X}_e)z \tag{51}$$

$$\dot{z} = v, \tag{52}$$

which is similar to system (27)–(28), except that now the first component has an asymptotically stable origin when the input is zero. In order to design  $v$  such that it stabilizes the overall system, we consider the candidate Lyapunov function  $V_o(\mathbf{X}_e, z)$  such that

$$V_o(\mathbf{X}_e, z) = V(\mathbf{X}_e) + \frac{1}{2}z^2. \quad (53)$$

The derivative of  $V_o$  is then

$$\dot{V}_o = \frac{\partial V}{\partial \mathbf{X}_e} \dot{\mathbf{X}}_e + \frac{\partial V}{\partial z} \dot{z} = \frac{\partial V}{\partial \mathbf{X}_e} (f(\mathbf{X}_e) + g(\mathbf{X}_e)\varphi) + \frac{\partial V}{\partial \mathbf{X}_e} g(\mathbf{X}_e)z + z\dot{z}. \quad (54)$$

Replacing the first term on the right hand side and  $\dot{z}$  by  $\dot{V}(\mathbf{X}_e)$  (see (38) and (52), respectively), yields

$$\dot{V}_o = \dot{V}(\mathbf{X}_e) + \frac{\partial V}{\partial \mathbf{X}_e} g(\mathbf{X}_e)z + z\nu.$$

Choosing  $\nu$  such that

$$\nu = -\frac{\partial V}{\partial \mathbf{X}_e} g(\mathbf{X}_e) - k_2 z, \quad k_2 > 0, \quad (55)$$

yields

$$\dot{V}_o = \dot{V}(\mathbf{X}_e) - k_2 z^2 \leq 0. \quad (56)$$

We have already shown that asymptotic stability at the origin of the subsystem (37) is achieved using  $\dot{V}(\mathbf{X}_e)$ ; thus, the origin ( $\mathbf{X}_e = \mathbf{0}, z = 0$ ) of system (51)–(52) is asymptotically stable. Since  $\varphi(\mathbf{0}) = 0$  we conclude that the origin ( $\mathbf{X}_e = \mathbf{0}, \zeta_e = 0$ ) is also asymptotically stable. Substituting (26), (43), and (46) we have

$$\nu = -x_{e2} - k_2(\zeta_e + x_{e1} + k_1 x_{e2}). \quad (57)$$

The state feedback control law is then

$$u = \dot{\varphi} + \nu. \quad (58)$$

Finally, by substituting (50) and (57) into (58) we obtain the exact control law given in (36).  $\square$

The resultant state feedback control law  $u$  is a function of the parameters  $x_{e1}$ ,  $x_{e2}$  and  $\zeta_e$ , where  $\mu_v$  and  $M$  are system constants. The control gains  $k_1$  and  $k_2$  should be chosen such that the control law will remain within the saturation boundaries of the valve's input  $u_V$ . Since the equilibrium point at the origin ( $\mathbf{X}_e = \mathbf{0}, \zeta_e = 0$ ) is asymptotically stable,  $u$  is guaranteed to drive an asymptotic convergence of the position error  $x_{e1}$  to the origin. In other words, the actuator's position  $x_1$  converges to the desired reference position  $x_d$  asymptotically and trajectory tracking is achieved. However, considering the original actuator system (14)–(15), we notice that there are two singular points at  $x_1 = 0$  and  $x_1 = l$ . Therefore, according to Lyapunov's stability theory, only a local (i.e.,  $0 < x_1 < l$ ) asymptotic stability is guaranteed.

## 5. Simulations

### 5.1. The Potential Energy Behavior

The potential energy significantly affects the behavior of the system and its stability. In order to acquire some insight into the behavior of the potential energy we performed simulations by solving numerically the potential energy equation (9) for the whole range of the actuator piston stroke ( $0.001 < x < 0.299$  m). The simulation results in Fig. 5 indicate that the potential energy behaves as a positive quadratic function with a global minimum,  $\mathcal{V}_{min}$ . This minimum is a stable equilibrium point of (9). The horizontal location of  $\mathcal{V}_{min}$  for the given parameters is at  $x = x_{min} = 0.1503$  m (i.e.  $\mathcal{V}(x_{min}) = \mathcal{V}_{min}$ ). Other parameters in this simulation were: the specific gas constant of air  $R = 287 \frac{\text{J}}{\text{kg K}}$ , the temperature  $T = 298$  K, the masses of air in the chambers  $m_1 = m_2 = 5e^{-4}$  kg, the piston cross sections  $A_1 = 3.1e^{-3}$  and  $A_2 = 2.8e^{-3}$  m<sup>2</sup>, and the dead volume  $V_0 = 18e^{-6}$  m<sup>3</sup>. Notice that choosing different masses  $m_1$  and  $m_2$  will affect the horizontal location of  $x_{min}$ .<sup>2</sup>

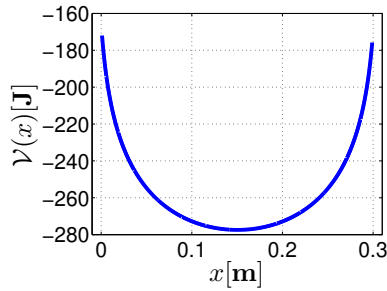


**Figure 5** The potential energy of the actuator  $\mathcal{V}$  as a function of the displacement  $x$

### 5.2. Dynamic Model Analysis

To analyze the behavior of the dynamic model we first find the equilibrium point  $\bar{x}$ . Solving the equation of motion (13) for  $\ddot{x} = \dot{x} = 0$ , results in

$$\bar{x} = \frac{m_1 l}{m_1 + m_2}. \quad (59)$$

Substituting the masses  $m_1$  and  $m_2$  according to (3) and the volumes according to (7) and (8), gives

$$\bar{x} = \frac{P_1 A_1 x l}{P_1 A_1 x + P_2 A_2 (l - x)} \quad (60)$$

where  $x$  is the current position of the piston defining the mass volume. With this volume and the pressure, letting go of the piston will lead the piston to the

<sup>2</sup>The specific vertical location of  $\mathcal{V}_{min}$  is a result of the chosen conditions. Generally, the potential energy,  $\mathcal{V}$ , is defined as a scalar quantity that depends on absolute physical quantities, such as the temperature, the mass, and the specific gas constant. Since these physical quantities are historically (or arbitrarily) pre-scaled according to international standards, and since energy is defined as a positive quantity with its theoretical minimum at zero, the vertical location of  $\mathcal{V}_{min}$  is not significant and can be shifted to any desired location on the vertical axis.

equilibrium point  $\bar{x}$ . For example, assigning values  $P_1 = 1.37$  bar,  $P_2 = 0.76$  bar,  $x = 0.1$  m,  $A_1 = 3.1e^{-3}$  m<sup>2</sup>,  $A_2 = 2.8e^{-3}$  m<sup>2</sup> and  $l = 0.3$  m, results in an equilibrium point which is located at  $\bar{x} = 0.15$  m.

Next, we plot in Fig. 6 the phase portrait for the initial state  $x = 0.1$  m and  $\dot{x} = 1$  m/s. The phase portrait is an illustration of the solution of (13), in which we plot the velocity  $\dot{x}$  versus the position  $x$ . The required parameters are set to the values for the equilibrium point example above. For reference behavior, we added another phase portrait plot, of a frictionless actuator. Examining the results for the frictionless actuator, represented by the solid line, we notice that the image of a periodic solution in the phase portrait is a closed trajectory, which is usually called a periodic orbit or a closed orbit. The equilibrium, however, is not asymptotically stable, since trajectories starting near the equilibrium point do not converge on it [15]. This periodic orbit is a result of a constant energy level which does not dissipate, since there is no friction. When friction is taken into consideration (the dashed line), trajectories starting close to the equilibrium point converge to it as time tends to infinity. Therefore we conclude that  $(\bar{x}, \dot{\bar{x}}) = (0.15, 0)$  is an asymptotically stable equilibrium point of the actuator. Finally, verification

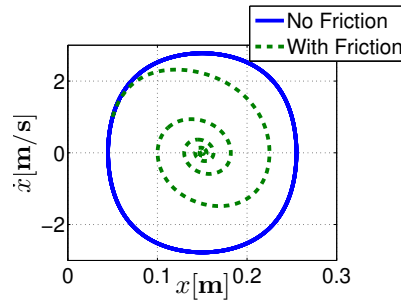


**Figure 6** The phase portrait of the actuator, with and without friction

of the derived equation of motion (13) is obtained by comparing it to the standard equation of motion, as derived from Newton's second law. By replacing the term  $-RT \left( \frac{m_1}{x} - \frac{m_2}{l-x} \right)$  according to (3), we get the standard equation of motion familiar from conventional studies

$$M\ddot{x} - P_1A_1 + P_2A_2 = -\mu_v\dot{x}.$$

## 6. Experiments

### 6.1. Test Setup

The dynamic model and control law were validated on a designated test setup, which is seen in Fig. 7. The test setup comprises a double-sided, single-ended piston rod type pneumatic actuator. In our experiments we used the BACCARA GEVA S3000 actuator with a cylinder bore diameter of 0.063m, a 0.02m diameter rod and a 0.3m stroke. The actuator is pneumatically connected, by two tubes, to a 5/3 proportional directional control valve of the Festo MPYE series. The valve controls the flow in and out of the actuator. The valve is controlled by an analog

signal of 0-10V, and is also connected to a pneumatic source providing a clean and dry supply of air at a semi-steady pressure of  $500 \div 700$ kPa. A Celesco SP1 potentiometer measures the position of the rod, and two SMC ISE30 series pressure gauges measure the pressure on both sides of the actuator. An 8-bit micro-controller (ARDUINO UNO) acquires data from the sensors at a sampling frequency of 1kHz. The control input signal is calculated and sent to the valve at a frequency of 0.1kHz, which is the bandwidth of the valve. An external mass (weights) is mounted on a linear slide rail. The total mass of the piston, the rod and the weights is 7.5kg. The slide rail is connected to a guided spring, which exerts a varying external force on the actuator.

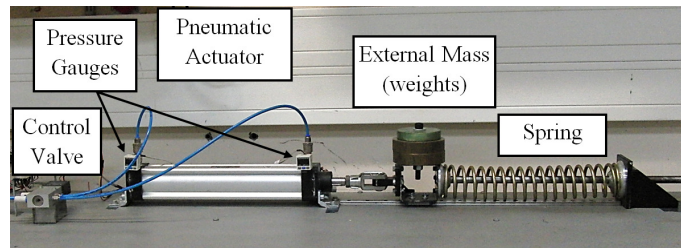


**Figure 7** Image of the test setup: the actuator is connected to a slider on a rail. The external mass is mounted on the slider, which is connected to a guided spring. The spring is fixed on the right side

## 6.2. *Dynamic Model Validation*

We validated the dynamic model by comparing the simulation and experimental results for the actuator. The experiment was configured such that the actuator is not subjected to any external force (the spring was taken off) and was moved from side to side with a total displacement of 0.2m; the velocity increased in accordance with the valve input. Figure 8 displays the actuator position (top), the valve input (middle) and the error of the model (bottom). At an input voltage of 5V the valve blocks the flow. As the input increases/decreases from this value, the flow-rate increases and, hence, the actuator opens/closes more quickly. The pressure and position measured during the experiment are used for calculating the mass of air inside the actuator's chambers. The simulation only relates to the actuator dynamics and does not include the air mass flow rate dynamics. Thus, the simulation input is the air masses and the output is the actuator's position. According to the simulation result, the root mean square error (RMSE) of the position is 0.002m in the model and the maximum error is  $\pm 0.004$ m.

## 6.3. *Tracking Performance*

To test the controller performance, we conducted two experiments. In one, the position trajectory was a square wave and in the other, it was a sinusoidal wave. The objective of the experiment was to test the controller accuracy under a disturbing force. The accuracy is measured by the tracking error, which is the difference between the position measured in the experiment and the position reference. A dis-

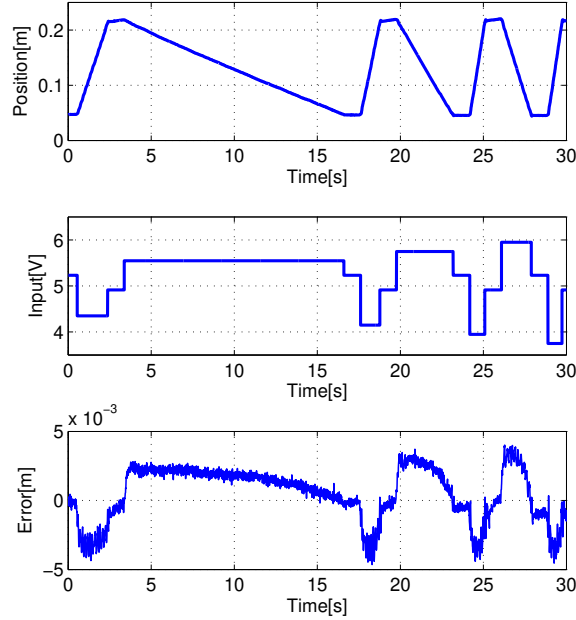


**Figure 8** Model validation: actuators position trajectory recorded in the experiment (top), valve input (middle) and model error (bottom)

turbance of an unknown varying external force is applied by the integration of a spring into the test setup. The magnitude of the generated force was varied as a function of the opening of the actuator. Since the opening is a function of time, the force is also time varying. The force was not modeled, i.e., it has no representation in the dynamic model and was not directly measured, although it affects the pressure inside the actuator's chambers.

Calculation of all the parameters in the control law (36) was performed as follows. The position error  $x_{e1}$  was calculated by (29), where the real position  $x_1$  was measured in real time. The desired position  $x_d$  is a system input signal which, in our system, is bounded such that  $0.05 \leq x_d \leq 0.25\text{m}$ .<sup>3</sup>

The velocity error  $x_{e2}$  was calculated by (30), where  $x_2$  is the time derivative of  $x_1$ , which was calculated by a first order numerical derivative and filtered by first order FIR filter.  $\dot{x}_d$  is the time derivative of the desired position  $x_d$ .  $\zeta_e$  was calculated from (31), which requires the real time data of the air mass  $m_1$  and  $m_2$  and the real

<sup>3</sup>A typical design of large pneumatic actuators includes a stroke cushioning on both ends of the actuator's cylindrical cover. This cushioning is designated to bring the piston and the mass to a smooth gentle halt against the end cover of the cylinder [16]. That is, the actuator dynamics change when the piston enters the cushioning band. In order to avoid the cushioning disturbance to the motion of the actuator's piston, the cushioning band in the tested actuator is taken to be 0.05m on both sides. This band is longer than the actual designed cushion band, but it guarantees that  $x_d$  remains inside the cushion free stroke.

time air mass flow rate  $\dot{m}_1$  and  $\dot{m}_2$ . The masses  $m_1$  and  $m_2$  were calculated by the ideal gas law (3), with real time measurements of the pressures,  $P_1$  and  $P_2$ , respectively, while the volumes  $V_1$  and  $V_2$  were calculated using the measured position  $x_1$ . The mass flow rates of air  $\dot{m}_1$  and  $\dot{m}_2$  were calculated from (20) and (21), respectively. The corresponding mass flow rate parameters  $\alpha_1 = -\alpha_2 = -0.004736\text{kg/s V}$  and  $\beta_1 = \beta_2 = 0.0005\text{kg/s}$  were found experimentally. The controller gains were set in the simulation such that the input cannot exceed the valve's input limitations, and fine tuned experimentally thereafter. In our experiments we set  $k_1 = k_2 = 5$ .

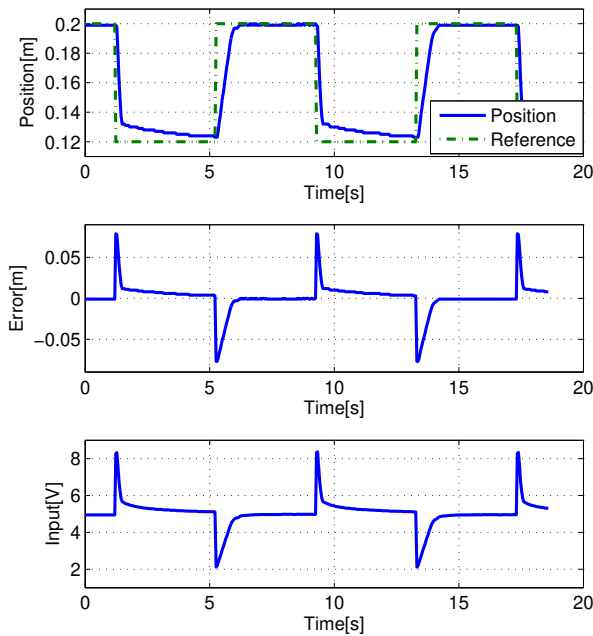


**Figure 9** Square wave tracking test: reference signal and measured position (top), tracking error (middle) and valve input (bottom)

The test results from tracking a square wave trajectory are shown in Fig. 9. The trajectory of the reference signal, with an amplitude of 0.08m, and the actuator recorded position are shown in the top trace. The faster response in the closing direction is in agreement with the increase in the magnitude of the force. The tracking error and the valve input are shown in the middle and the bottom traces, respectively. Due to a significant asymmetry in the error behavior we mention two error values: the upper step RMSE is 0.02m and the lower step RMSE is 0.016m. Although the steady state error of the lower step is considerably larger than for the upper step, the upper RMSE is greater. This is a consequence of the increasing resistance of the spring in the upper step, while in the lower step the force acts in the direction of the movement. Inspection of the corresponding input reveals that, although appropriate input is received, the steady state error is reduced very

slowly. We conclude that this behavior is due to poor operation of the valve in the neighborhood of 5V.

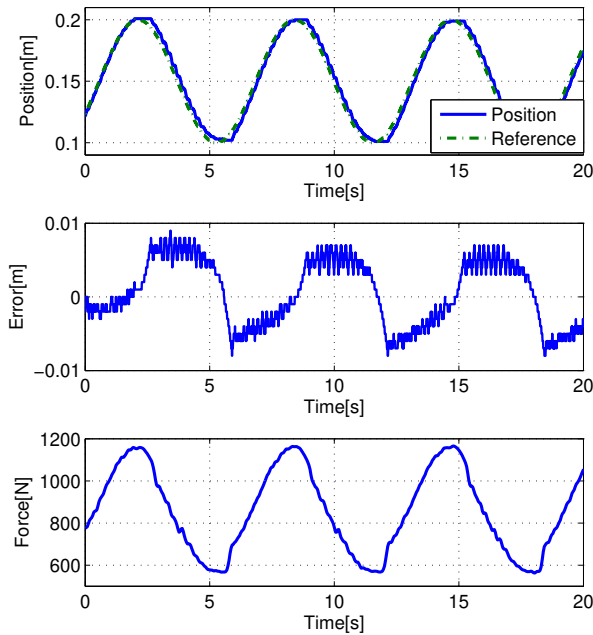


**Figure 10** Sinusoidal wave tracking test: reference signal and measured position trajectories (top), tracking error (middle) and estimated external force (bottom)

The test results from tracking the sinusoidal wave are shown in Fig. 10. The trajectory of the reference signal, with an amplitude of 0.1 m, and the actuator recorded position are shown on the top. The tracking error, shown on the middle, is within  $\pm 0.008$  m and the RMSE is 0.004 m. In contrast to the square wave test, the external force and its varying magnitude are hardly noticed. The bottom trace shows the estimation of the external force in this experiment. The magnitude of the external force, which varies from 570 N to about 1150 N, constitutes a significant disturbance to the actuator, considering it can produce a maximum force of about 1600 N in the given configuration.

## 7. Conclusions

This paper presents a novel position control law for a pneumatic actuation system, which continues to perform accurately when subjected to a disturbance due to an external force. A new modeling approach was used to derive the dynamic model of the actuator. Based on energy principles, the Lagrangian of the actuator was introduced as a preliminary step towards the derivation of the equation of motion. Simulation of the dynamic model showed good correspondence with experimental

results. The nonlinear backstepping method was applied in order to design a stabilizing state feedback control law. Tracking is achieved by introducing the error vector, which includes the zeta error, as the state vector. The advantage of this control law is that, even though the actuator is disturbed by a time varying external force, the tracking performance is not affected. In future work, we will focus on the bounds for the dynamic model and disturbance uncertainty. Further, we will consider the development of a method to automatically calculate optimal  $k_1$  and  $k_2$  gains and also will extend the simulation to include the air mass flow rate model.

## References

- [1] **Shearer, J.L.:** *Continuous control of motion with compressed air*, Ph.D. Thesis, Massachusetts Institute of Technology, **1954**.
- [2] **Richer, E. and Hurmuzlu, Y.:** A high performance pneumatic force actuator system: Part II - Nonlinear controller design, *Journal of Dynamic Systems, Measurement, and Control*, **122**, 426–434, **2000**.
- [3] **Liu, S. and Bobrow, J.E.:** An Analysis of a Pneumatic Servo System and Its Application to a Computer-Controlled Robot, *Journal of Dynamic Systems, Measurement, and Control*, **110**, 228–235, **1988**.
- [4] **Lai, J.Y., Menq, C.H. and Singh, R.:** Accurate position control of a pneumatic actuator, *Journal of Dynamic Systems, Measurement, and Control*, **112**, 734–739, **1990**.
- [5] **Ben-Dov, D. and Salcudean, S.E.:** A force-controlled pneumatic actuator, *IEEE Trans. Robot. and Autom.*, **11**(6), 906–911, **1995**.
- [6] **Rao, Z. and Bone, G.M.:** Modeling and control of a miniature servo pneumatic actuator, in: *Proc. 2006 IEEE Robotics and Automation Conf., Orlando, FL, USA*, 1806–1811, **2006**.
- [7] **Smaoui, M. and Brun, X. and Thomasset, D.:** A study on tracking position control of an electropneumatic system using backstepping design, *Control Engineering Practice*, **14**, 923–933, **2006**.
- [8] **Hodgson, S. et al.:** Sliding-mode control of nonlinear discrete-input pneumatic actuators, in: *2011 IEEE/RSJ Int. Conf. Intelligent Robots and Systems*, San Francisco, CA, USA, 738–743, **2011**.
- [9] **Shtessel, Y. and Taleb, M. and Plestan, F.:** A novel adaptive-gain super-twisting sliding mode controller: Methodology and application, *Automatica*, **48**, 759–769, **2012**.
- [10] **Taleb, M. and Levant, A. and Plestan, F.:** Pneumatic actuator control: Solution based on adaptive twisting and experimentation, *Control Engineering Practice*, **21**, 727–736, **2013**.
- [11] **Lu, C.H. and Huang, Y.R. and Shen, Y.T.:** Backstepping sliding-mode control for a pneumatic control system, in: *Proc. Institution of Mechanical Engineers, Part I: Journal of Systems and Control Engineering*, **224**, 763–770, **2010**.
- [12] **Elleuch, D. and Damak, T.:** Backstepping sliding mode controller coupled to adaptive sliding mode observer for interconnected fractional nonlinear system, *Int. J. Recent Advances in Telecommunications, Signals and Systems*, **75**, 130–138, **2013**.
- [13] **Osuka, K. and Kimura, T. and Ono, T.:** H-infinity control of a certain nonlinear actuator, in: *Proc. 29th IEEE Conf. Decision and Control, Honolulu, HI, USA*, 370–371, **1990**.

- [14] **Jeltsema, D. and Scherpen, J.M.A.:** Multidomain modeling of nonlinear networks and systems, *IEEE Control Syst. Mag.*, **29**, 28–59, **2009**.
- [15] **Khalil and Hassan K.:** *Nonlinear Systems*, 3rd ed., Prentice-Hall, New Jersey, **2002**.
- [16] **Beater, P.:** *Pneumatic Drives*, Springer, Berlin, **2007**.